ACS Photonics

pubs.acs.org/journal/apchd5

Article

Dual-Polarization Topological Interface States in Ridge Photonic Crystals

Ze-Ming Chen, Lu-Hang Jin, Weimin Deng,* Wenjie Chen,* Shaoji Jiang, and Jianwen Dong

Cite This: https://doi.org/10.1021/acsphotonics.4c00248

Read Online

ACCESS | Metrics & More | Article Recommendations | Supporting Information

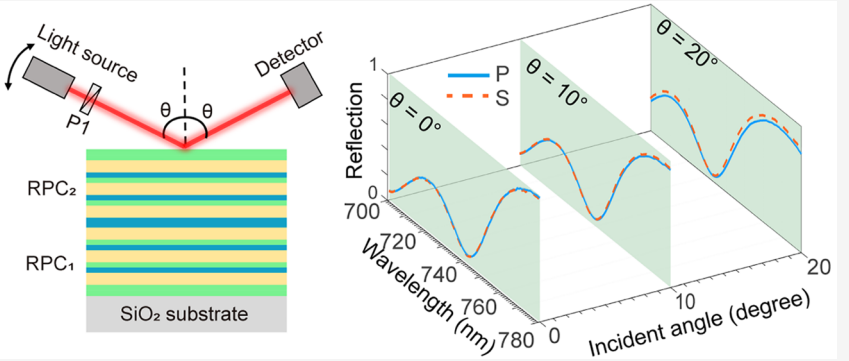

ABSTRACT: Lifting the nodal ring degeneracy can result in topologically nontrivial ridge bulk states and associated interface states, which have been realized by 1D photonic crystals. However, the ridge interface states exist only for p polarization, which limits their potential applications in polarization-independent optical devices. Here, a scheme to design the polarization-independent nodal ring using a 1D photonic crystal is proposed. It is revealed that the fourfold degeneracy exactly lies at the position where the absentee layer condition is satisfied for each layer. Once the absentee layer condition cannot be satisfied for each layer, the nodal ring will be gapped, accompanied by ridge interface states traversing the gap. Interestingly, these p-polarized and s-polarized ridge interface states are degenerate almost in the whole band gap, which facilitates polarization-independent optical filtering. This work proposes a novel way for polarization-independent optical filtering and associated applications, such as high-efficiency solar energy conversion and privacy screen.

KEYWORDS: *ridge photonic crystals, nodal ring, topological interface states, dual polarization*

INTRODUCTION

Photonic topological states in three-dimensional (3D) momentum space possess rich physical properties and interesting phenomena,[1,2] such as robust surface transport[3,4] and negative refraction of surface waves.[5,6] In general, the 3D topological states can be divided into two classes. One of them is the gapped topological states,[7−9] such as 3D photonic topological insulators.[4,10] Another class is the gapless topological states[11−18] (i.e., photonic topological semimetals), such as nodal rings[19,20] (a ring-shaped line degeneracy). Topological semimetals can serve as the parent states of various kinds of gapped topological states and have attracted much interest. For example, by breaking the symmetry of the system, a nodal ring degeneracy can transit to a topologically nontrivial ridge state.[21,22] So far, researchers have successfully observed the nodal ring degeneracy in metallic photonic crystals (PCs) and metacrystals.[19,23] However, these carefully designed artificial periodic structures are usually very complex, hindering their applications in nanoscale photonic systems.

To overcome these issues, researchers have started to explore the topological nodal ring degeneracy in simple structures. In theory, researchers have pointed out that a 2-fold degenerate nodal ring can exist in a 1D PC composed of anisotropic dielectrics[24] or design various types of 4-fold degenerate nodal ring by a 1D hypercrystal.[25] Recently, researchers have experimentally demonstrated that a 4-fold degenerate nodal ring can be realized simply by a 1D PC composed of isotropic dielectrics.[26] Meanwhile, we have experimentally observed a 2-fold degenerate nodal ring in a 1D dielectric PC and the associated ridge interface states by lifting the nodal ring degeneracy.[22] However, these ridge interface states exist only for p polarization, which imposes constraints on their potential applications in polarization-independent optical filters and associated devices.

Received: February 7, 2024
Revised: May 15, 2024
Accepted: May 16, 2024

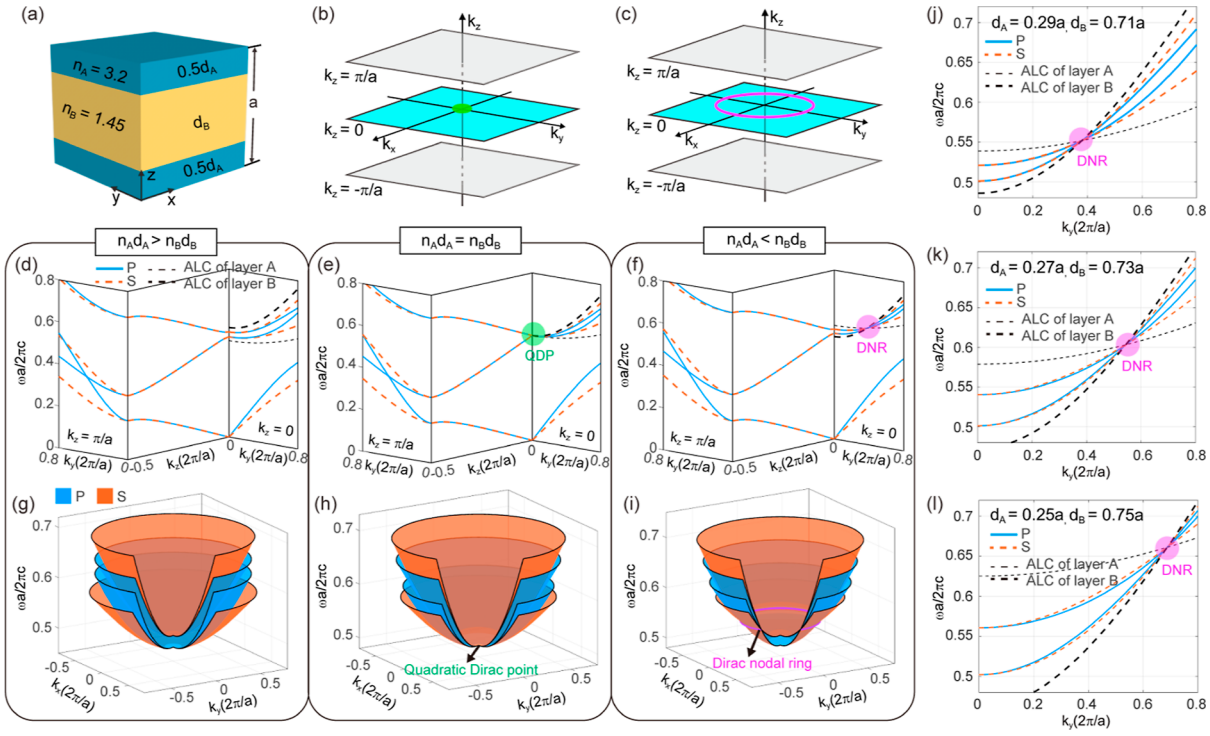

Figure 1. Design of dual-polarization DNR in a 1D PC. (a) Inversion symmetric unit cell of a 1D PC, which consists of three dielectric layers (A/B/A). The refractive index and thickness of layer A (B) are 3.2 (1.45) and d_A (d_B), respectively. (b,c) 3D Brillouin zone of the 1D PC. The cyan plane highlights the k_x−k_y plane at $k_z = 0$. The green circle in (b) marks the position of a QDP. The purple circle in (c) marks a dual-polarization nodal ring. (d) P-polarized (light-blue solid lines) and s-polarized (orange dashed lines) band structures along the k_z and k_y directions when $d_A = 0.34a$ and $d_B = 0.66a$. The black thin dashed line and thick dashed line represent the absentee layer condition for layer A and layer B, respectively. There is not any 4-fold degenerate point in the band structures. (g) 3D band structures on the $k_z = 0$ plane. For a better view of the degeneracy, only three-quarters of the bands are shown. (e,h) Similar to (d) and (g), but for the case of $d_A = 0.3118a$ and $d_B = 0.6882a$. In this case, the quarter-wave stack condition $n_A d_A = n_B d_B$ is satisfied. The green circle highlights the QDP. (f,i) Similar to (d) and (g), but for the case of $d_A = 0.29a$ and $d_B = 0.71a$. The purple circle highlights the position of DNR. (j) Band along k_y direction when $d_A = 0.29a$ and $d_B = 0.71a$. (k,l) Similar to (j) but for the case of $d_A = 0.27a$, $d_B = 0.73a$ and $d_A = 0.25a$, $d_B = 0.75a$, respectively.

In this work, starting from a quarter-wave stack, a method to design a dual-polarization nodal ring in a 1D PC is proposed. We reveal that the existence of these fourfold degeneracies can be understood from the perspective of absentee layer conditions in thin-film optics. By changing the refractive index of one layer in the unit cell, the absentee layer condition cannot be simultaneously satisfied for each layer, so that the nodal ring will be gapped and transit to nontrivial ridge states, manifested as localized Berry vortexes. The existence of dual-polarization ridge interface states is experimentally observed, and we find that p-polarized and s-polarized interface bands are degenerate almost in the whole band gap. Our work makes it possible to realize a polarization-independent optical filter and associated devices using 1D PCs.

RESULTS AND DISCUSSION

Although a nodal ring for single polarization (based on the principle of Brewster angle, a single-polarization effect) has been reported in ref 22, the present work studies the dual-polarization nodal ring and relevant topological interface states. Note that a prerequisite for dual-polarization ridge states is the existence of a dual-polarization nodal ring. It seems that a simple way to achieve a dual-polarization nodal ring is to fine-tune the structural parameters of 1D PCs to have an accidentally double-degenerate nodal ring, e.g., by using dual-symmetric ($\varepsilon = \mu$) materials. But this is unrealistic for most natural materials. Here, we start by introducing the method to design a dual-polarization nodal ring using all-dielectric materials. We consider a 1D PC consisting of alternating layer A ($n_A = 3.2$) and layer B ($n_B = 1.45$), as shown in Figure 1a. Their thicknesses are d_A and d_B, respectively. Apart from Bloch wavevector k_z, we take in-plane components k_x and k_y into account to construct a 3D momentum space. The 3D Brillouin zone of this 1D PC is bounded only in the k_z-direction by two planes of $k_z = \pm \pi/a$ because this 1D PC has discrete translational symmetry only in the z-direction, as shown in Figure 1b. Besides, such 1D PC is isotropic and has continuous translational symmetry on the xy-plane, indicating that its dispersion relations along any radial direction are identical. Based on this special property, a fourfold degenerate nodal ring will emerge on the k_x−k_y plane if one can realize a fourfold degenerate point along any radial direction (say, k_y direction). In order to realize the above scheme, we start from the case of a quarter-wave stack, i.e., $n_A d_A = n_B d_B$. Figure 1e shows the s-polarized (dashed orange lines) and p-polarized (solid blue lines) bands along the k_z direction and k_y direction. In the band structure along the k_z direction ($k_y = 0$), s-polarized and p-polarized bands are degenerate due to rotational symmetry. Furthermore, one can see that the second photonic band gap vanishes at $k_z = 0$ (highlighted by the green circle).[27] This special property induces a fourfold degenerate point at the Γ point. Figure 1h shows the 3D band structures on the $k_z = 0$ plane. For a better view of the degeneracy, only three-quarters of the bands are shown. One can see that the

https://doi.org/10.1021/acsphotonics.4c00248
ACS Photonics XXXX, XXX, XXX−XXX

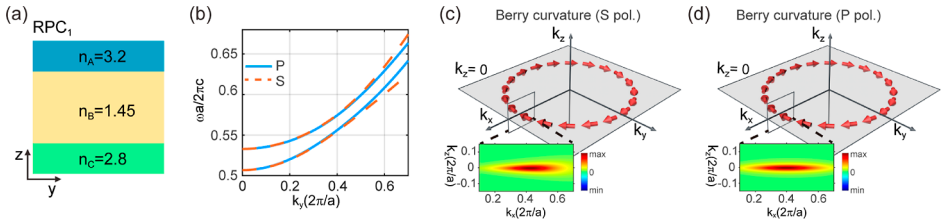

Figure 2. Dual-polarization ridge photonic crystals. (a) Unit cell of dual-polarization RPC_1. (b) Bulk band structure of RPC_1 along the k_y direction. Note that a partial gap opened in the vicinity of the original nodal ring. (c,d) Localized Berry vortexes for (c) s-polarized and (d) p-polarized lower bands in (b). The insets show the cross-sectional views of the Berry curvature.

fourfold degenerate point is actually a quadratic Dirac point (QDP).[28] Then, we can deform this QDP into a Dirac nodal ring (DNR) by breaking the quarter-wave stack condition. To be specific, we change the thickness of each layer so that the quarter-wave stack condition is not satisfied any more, i.e., $n_A d_A > n_B d_B$ or $n_A d_A < n_B d_B$. For the case of $n_A d_A > n_B d_B$, we choose a 1D PC with $d_A = 0.34a$ and $d_B = 0.66a$ as an example. Figure 1d shows the calculated band structure of this 1D PC. Compared with Figure 1e, the original fourfold degeneracy is lifted and a band gap emerges. On the other hand, for the case of $n_A d_A < n_B d_B$, we choose $d_A = 0.29a$ and $d_B = 0.71a$ as an example. As highlighted by the purple circle in Figure 1f, the original four-band crossing point at $k_y = 0$ is moved to $k_y = 0.38 \times 2\pi/a$. Since the 1D PC is rotation invariant on the xy-plane, this fourfold degenerate point extrudes along the azimuthal direction, forming a ring of double Dirac points [purple in Figure 1i]. For the dual-polarization DNR, its effective Hamiltonian can be written as

$$H = [v_x q_z \sigma_x + (v_0\sigma_0 + v_z\sigma_z)q_r]\tau_0 \tag{1}$$

where σ_i is the Pauli matrix, τ_0 is the identity matrix, and q_z and q_r represent the normalized wavevector along z and radial directions, respectively (see more details in Note S6). Here, τ_0 acts on the pseudospin (i.e., polarization) subspace. For each polarization, the effective Hamiltonian resembles a type-II Weyl nodal ring's Hamiltonian, indicating that it carries the π Berry phase.[29] In a condensed matter system, nodal rings are sensitive to spin−orbit coupling because spin−orbit coupling can induce hybridization between opposite spin components.[30] In our photonic system, the polarization degree of freedom, rather than spin, is used to construct a double nodal ring. The coupling between s- and p-polarized states is naturally avoided. Since 1D PC possesses continuous rotational symmetry in the $x-y$ plane, one can always define two sets of decoupled modes (s polarized and p polarized). Therefore, the usual sensitivity of nodal rings to spin−orbit coupling is avoided in this work.

This double nodal ring is actually composed of two single nodal rings (for p and s polarizations) occurring exactly at the same momentum and frequency. The existence of these 4-fold degeneracies (QDP and DNR) can be explained by the absentee layer condition in thin-film optics. The characteristic matrix of each layer can be expressed as[31,32]

$$M_j = \begin{bmatrix} \cos\delta_j & i\sin\delta_j/\eta_j \\ i\,\eta_j\sin\delta_j & \cos\delta_j \end{bmatrix} \tag{2}$$

where j = A or B. δ_j and η_j are the phase thicknesses and optical admittances of each layer. The phase thickness is defined as $\delta_j = k_0\, n_j d_j \cos(\theta_j)$, in which n_j and d_j are the refractive index and thickness of each layer; and θ_j and k_0 are the refraction angle and wavenumber in vacuum. Optical admittance is expressed as $\eta_j = n_j/\cos(\theta_j)$ for s polarization and $\eta_j = n_j/\cos(\theta_j)$ for p polarization. When the phase thickness of one layer is integer times π ($\delta_j = m\pi$), it is an absentee layer for the waves at that frequency. In this case, the characteristic matrix in eq 2 becomes an identity matrix, which means that the existence of the absentee layer should not affect the reflectance or transmittance as if it is absent. Especially, when both layer A and layer B satisfy absentee layer condition (i.e., $\delta_A = m_1\,\pi$ and $\delta_B = m_1\,\pi$) at some frequency and some k_r, the whole crystal is effectively absent for both polarization waves, resulting in band gap closing and a 4-fold degeneracy. Note that this statement from the perspective of absentee layer condition coincides with the double nodal ring conditions provided in ref 26, which explains the existence of the dual-polarization nodal ring by the requirement on the ratio between two layers' optical paths. Based on this condition, we can design a dual-polarization nodal ring at any specific ω and k_r. Using the relation $k_r = n_j k_0 \cos(\theta_j)$, we have the phase thickness $\delta_j = k_0 d_j \sqrt{n_j^2 - k_r^2/k_0^2}$. After some algebra, the absentee layer condition reads

$$\left(\frac{\omega a}{2\pi c}\right)^2 - \left(\frac{k_r a}{2\pi n_j}\right)^2 = (ma/2n_j d_j)^2 \tag{3}$$

We plot the $\omega - k_r$ hyperbolas at which the absentee layer condition is satisfied, with black thin (thick) dashed curves for layer A (B) in Figure 1d−f. From Figure 1e,f, it is clear that the black thin dashed curve and the black thick dashed curve exactly cross at the 4-fold degenerate point. Besides, we emphasize that eq 3 provides a clear guidance to tune the position of these 4-fold degenerate points. According to eq 3, one can tune the cross position or even remove the crossing point of these curves by tuning the refractive index or layer thickness of each layer. It should be noted that the physical mechanism in this work is different from that in ref 22. The single nodal ring in ref 22 is due to the p-polarized band gap closing at the Brewster angle between two constituent dielectrics. Note that the Brewster effect is polarization dependent and a similar total transmission phenomenon does not occur for s polarization, regardless of the structural/material parameters, unless considering magnetic materials with $\mu_r \neq 1$. Thus, a dual-polarization nodal ring cannot be achieved by simply tuning 1D PC's parameters. Here, the scheme to achieve a dual-polarization nodal ring is based on the concepts of the absentee layer, which is a polarization-independent effect. Furthermore, this type of 4-fold degeneracy is robust against parameters' perturbations. Figure 1j−l shows the in-plane dispersions for three different filling ratios, where s- and p-polarized bands always cross at the same frequency and wavevector. It indicates that this is not an

https://doi.org/10.1021/acsphotonics.4c00248
ACS Photonics XXXX, XXX, XXX−XXX

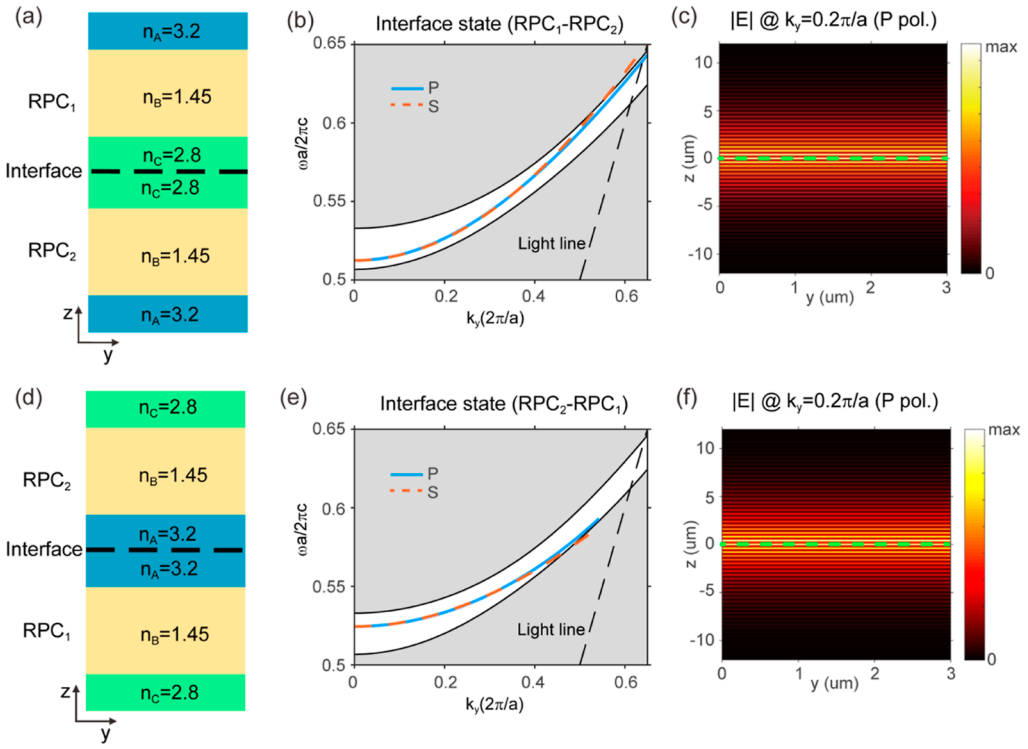

Figure 3. Dual-polarization ridge interface states. (a) Schematic of the RPC_1−RPC_2 domain wall. (b) P-polarized (light-blue solid lines) and s-polarized (orange dashed lines) projected bands of the RPC_1−RPC_2 domain wall. The dashed line represents the light line of air. Interface states emerge in the gap due to the opposite Berry vortexes of two RPCs. (c) Electric field's magnitude of the p-polarized ridge interface state at $k_y = 0.2\pi/a$. The green dashed line highlights the position of the interface. (d−f) Similar to (a−c), but for the RPC_2−RPC_1 domain wall.

accidental degeneracy by adjusting appropriate parameters. From the perspective of symmetry, this degeneracy between s-band crossing and p-band crossing is not guaranteed by spatial/time-reversal symmetry and is somewhat exotic. Usually, symmetry-protected degeneracy would happen along/on the symmetric k-line/plane. The absentee-layer-induced degeneracy only occurs at a nonsymmetric k_r or incident angle, while the s- and p-polarized bands split away from the crossing point with different slopes (group velocities).

Our previous work has demonstrated that the nodal ring can transit to topologically nontrivial ridge states by breaking inversion symmetry.[22] Here, we choose to replace the bottom layer A by a layer C with a refractive index of 2.8 (Figure 2a) and named it ridge photonic crystal1 (RPC_1). For RPC_1, since the absentee layer condition cannot be simultaneously satisfied for all three layers, the original double DNR degeneracy is lifted in Figure 2b. It should be noted that in ref 26, the authors focus on the study of gapless nodal ring states (without a topological band gap), rather than gapped ridge states. To investigate the topological property of these ridge bulk states, the Berry curvatures for the bands below the gap are calculated in Figure 2c,d for s-polarized and p-polarized bands. The insets show a zoomed-in view of the Berry curvature on the cut plane of $k_y = 0$, where Berry curvatures are localized around the $k_z = 0$ plane. A toroidal-shaped Berry flux flows in the counterclockwise direction for both polarizations. Alternatively, one can instead replace the top layer A by a layer C (named RPC_2). Because RPC_1 and RPC_2 are inversion partners of each other, they have identical bulk band dispersions, but the band topologies of RPC_1 and RPC_2 are different. Berry vortexes of RPC_2 flow in the opposite direction to that of RPC_1, see more details in Supplementary Figure S3.

In the 2D photonic system, Dirac cones can be gapped by inversion symmetry breaking, which results in the gapped photonic valley states.[33−36] Nodal rings can be deemed as the extrusion of 2D Dirac points along a closed loop. By breaking the nodal ring, the resulting ridge states can be considered as the 3D version of the valley states. Therefore, these opposite topological features of RPC_1 and RPC_2 guarantee the existence of the ridge interface state in the domain wall formed by RPC_1 and RPC_2. Note that researchers have studied interface states between 1D PCs and metals, which are well known as optical Tamm states.[37−39] The formation of an optical Tamm state can be attributed to the fact that the reflection phase of the metal (usually negative) exactly compensates with the one of 1D PC (positive). Likewise, the existence of ridge interface states between two topologically distinct RPCs is due to a similar resonance condition (see Figure S6). The only difference is that the compensation between RPC_1 and RPC_2 is guaranteed by their distinct Berry curvatures, which has been demonstrated in our previous work.[22] We first consider the RPC_1−RPC_2 domain wall, where RPC_1 is on the top of RPC_2, as sketched in Figure 3a. In the calculated projected bands of Figure 3b, two interface bands reside in the gap for both s polarization (orange dashed line) and p polarization (light-blue solid line). Note that the s-polarized and p-polarized ridge interface states propagate in the same direction because the Berry curvatures of the s-polarized band and p-polarized band flow in the same direction for RPC_1 (RPC_2). Moreover, the s-polarized and p-polarized ridge interface states are degenerate almost in the whole band gap, which is hard to realize in other dielectric waveguide systems, because optical material's response to electric field and magnetic field is usually different. Since the absentee layer conditions are broken for RPCs, the

https://doi.org/10.1021/acsphotonics.4c00248
ACS Photonics XXXX, XXX, XXX−XXX

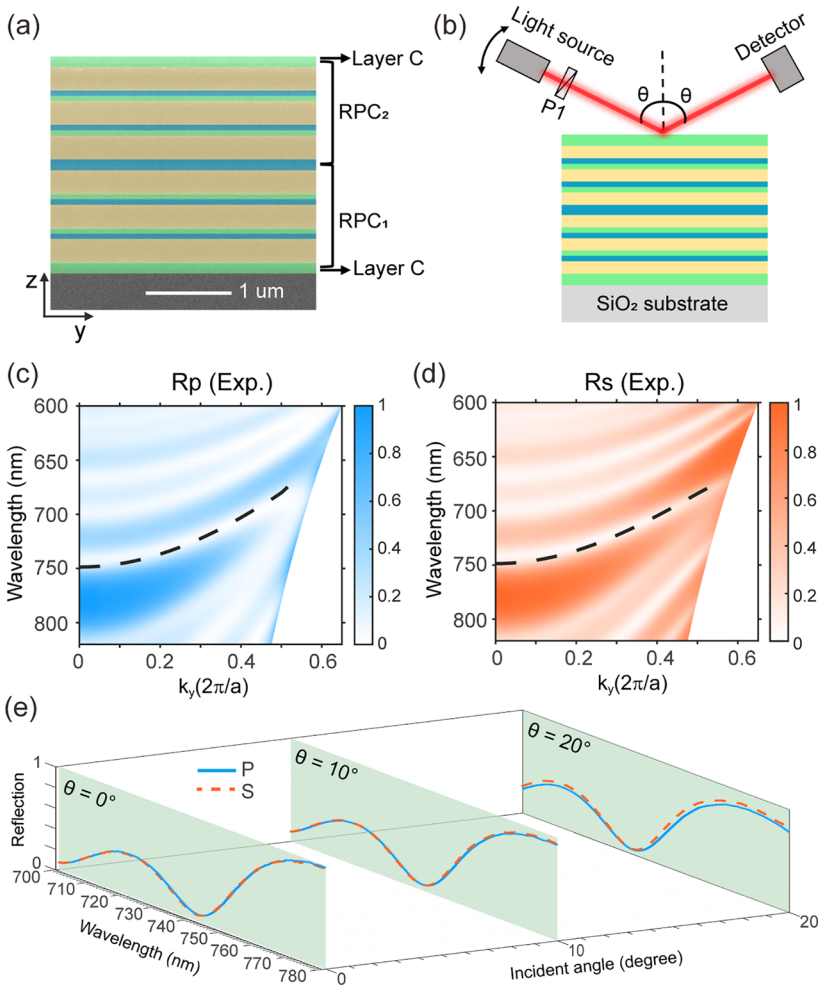

Figure 4. Experimental observation of dual-polarization ridge interface states. (a) Scanning electron microscopy image of the sample. (b) Experimental setup; P_1, polarizer. (c,d) Experimental measured angle-resolved reflection spectra for p polarization and s polarization. Calculated dispersions of ridge interface states (dashed lines) coincide with the reflection dips, demonstrating the existence of dual-polarization ridge interface states. (e) P-polarized (light-blue solid line) and s-polarized (orange dashed line) reflection spectra when the incident angle $\theta = 0°$, 10°, and 20°.

interface states are not exactly degenerate over the whole band gap. But thanks to the similar topological features (reflection phase winding) for s and p polarizations (see Figure S6), the s- and p-polarized interface bands are nearly degenerate in the whole band gap. As an example, Figure 3c shows the electric field of the p-polarized ridge interface state at $k_y = 0.2\pi/a$, where the green dashed line highlights the position of the interface. One can see that the electric field is tightly localized near the interface. Alternatively, one can also construct an interface by placing RPC_2 on the top of RPC_1, i.e., the RPC_2−RPC_1 domain wall [Figure 3d]. As expected, there are also interface states in the band gap for both polarizations; see Figure 3d. Similar to the dispersion of the RPC_1−RPC_2 domain wall, the s-polarized and p-polarized ridge interface states are also degenerate almost in the whole band gap. P-polarized and s-polarized interface states are degenerate in the frequency range (0.5125, 0.559)*c/a, with a relative bandwidth of 8.7%, which is beneficial for achieving a polarization-independent filter whose working frequency can be tuned in a wide frequency range by adjusting an appropriate incident angle.[40] Interestingly, these interface states carry transverse spin, which enable unidirectional excitation of interface states (see more details in Figure S5). Interface states of ridge photonic crystals can be modulated by using phase change materials[41] or soft materials.[42] Topologically protected interface states can survive even when the refractive indices of the materials deviate in a wide range, until the original DNR with finite radius shrinks to a point (see more details in Figure S4).

In order to observe dual-polarization ridge interface states in the experiment, we fabricated samples using an inductively coupled plasma-enhanced chemical vapor deposition (ICP-CVD) system (Oxford Instruments PlasmaPro System 100). Layer B is realized by depositing a SiO_2 film with a thickness of 274 nm. For layers A and C, we deposited two kinds of silicon-rich nitride films (SRN_1 and SRN_2) with a thickness of 61 nm. Different refractive indices of SRN can be achieved by tuning the ratio between SiH_4/N_2 during the deposition process. Optical constants of SRN_1 and SRN_2 are measured in Supplementary Figure S1. Figure 4a shows the scanning electron microscopy image of an RPC_2−RPC_1 domain wall, which is composed of 3-period RPC_2 and 3-period RPC_1. Besides, to avoid the disturbance from redundant trivial interface states [between RPC_2 and air, or between RPC_1 and substrate ($n = 1.45$)], two extra layers of layer C are added on the top and the bottom of the domain wall structure (see more details in Figure S2). To demonstrate the existence of a ridge interface state, angle-resolved reflection spectra of the sample were measured using the experimental setup in Figure 4b.

https://doi.org/10.1021/acsphotonics.4c00248
ACS Photonics XXXX, XXX, XXX−XXX

Figure 4c,d shows the measured reflection spectra for p and s polarization, respectively. High-reflectivity regions agree well with the projected band. Black dashed lines represent the calculated dispersion of the interface state. As expected, a line of reflection dip exists for both p-polarized and s-polarized spectra, confirming the existence of the ridge interface state.

Interestingly, from Figure 3e, we find that p- and s-polarized ridge interface states are degenerate in a broad frequency range. This can be utilized for the polarization-independent optical filter whose working frequency can be tuned in a wide range. For instance, we plot the reflection spectra when the incident angle $\theta = 0°$, 10°, and 20° in Figure 4e. In the case of $\theta = 10°$, the dips of p-polarized (light-blue solid line) and s-polarized (orange dashed line) reflection spectra both locate at the wavelength of 740 nm. Even when the incident angle varies from 10 to 20°, the dips in both spectra still locate at the same wavelength of 733 nm.

CONCLUSIONS

In conclusion, we point out that absentee layer conditions can provide clear guidance to design a dual-polarization nodal ring in a simple 1D PC. By perturbing the absentee layer condition, the gapless nodal ring states transit to nontrivial gapped ridge states. In the domain wall formed by two RPCs with opposite Berry vortexes, ridge interface states emerge for both polarizations, and they are degenerate almost in the whole band gap. Compared with the single-polarization ridge interface state, our scheme relaxes the polarization constraint and makes it possible to realize dual-polarization photonic devices based on 1D PC, such as polarization-independent angularly selective optical filters, which can be utilized for high-efficiency solar energy conversion[43,44] and privacy screen.[45] By stacking a series of similar 1D PCs with different scaling factors, a cascaded PC can serve as an angular filter, enabling high conversion efficiency and privacy screen.[46]

MATERIALS AND METHODS

Numerical Simulation. The bulk bands of 1D photonic crystals were calculated by MIT photonic bands (MPBs).[47] The interface states' dispersion and field patterns were calculated by COMSOL Multiphysics. All of the reflection spectra were calculated by the transfer matrix method.

Sample Fabrication. The sample shown in Figure 4a was fabricated by an ICP-CVD system (Oxford Instruments PlasmaPro System 100) on a quartz substrate. The deposition rate was 12.4 nm min^{-1} for the SiO_2 layer. The different refractive indices of SRN were achieved by changing the ratio of SiH_4/N_2 during the process of deposition. The deposition rate was 6.8 nm min^{-1} for the SRN_1 layer and 9.2 nm min^{-1} for the SRN_2 layer.

Optical Measurements. The refractive index and extinction coefficient of SRN1 and SRN2 were determined from spectrometry ellipsometry measurements (Sentech SE400). Angle-resolved reflection spectra of the sample were measured by an angle-resolved spectrometer (R1-UV, Ideaoptics, China).

ASSOCIATED CONTENT

Supporting Information

The Supporting Information is available free of charge at https://pubs.acs.org/doi/10.1021/acsphotonics.4c00248.

Optical constants of silicon-rich nitride, interface states residing in the RPC_2−air interface or RPC_1−substrate interface, bulk band and Berry curvature of RPC_2, interface states in the RPC_1−RPC_2 domain wall for n_c with different values, transverse spin in the interface states, effective Hamiltonian of dual-polarization Dirac nodal ring, and reflection phases of RPCs (PDF)

AUTHOR INFORMATION

Corresponding Authors

Weimin Deng − *School of Physics and Materials Science, Nanchang University, Nanchang 330031, China; School of Physics & State Key Laboratory of Optoelectronic Materials and Technologies, Sun Yat-sen University, Guangzhou 510275, China*; Email: dengweimin@ncu.edu.cn

Wenjie Chen − *School of Physics & State Key Laboratory of Optoelectronic Materials and Technologies, Sun Yat-sen University, Guangzhou 510275, China*; Email: chenwenj5@mail.sysu.edu.cn

Authors

Ze-Ming Chen − *School of Physics & State Key Laboratory of Optoelectronic Materials and Technologies, Sun Yat-sen University, Guangzhou 510275, China*

Lu-Hang Jin − *School of Physics & State Key Laboratory of Optoelectronic Materials and Technologies, Sun Yat-sen University, Guangzhou 510275, China*

Shaoji Jiang − *School of Physics & State Key Laboratory of Optoelectronic Materials and Technologies, Sun Yat-sen University, Guangzhou 510275, China*

Jianwen Dong − *School of Physics & State Key Laboratory of Optoelectronic Materials and Technologies, Sun Yat-sen University, Guangzhou 510275, China*; orcid.org/0000-0003-2379-554X

Complete contact information is available at: https://pubs.acs.org/10.1021/acsphotonics.4c00248

Author Contributions

Z.-M.C. and L.-H.J. contributed equally to this work. W.D. and W.C. conceived the idea. L.-H.J. and W.D. performed the numerical simulations. L.-H.J. derived eq 3. Z.-M.C. fabricated the samples. Z.-M.C. and W.D. performed the optical measurements. All authors contributed to the analysis of the results. W.D., W.C., S.J., and J.D. wrote the manuscript with input from other authors. W.C. and J.D. supervised the project. All authors have given approval to the final version of the manuscript.

Notes

The authors declare no competing financial interest.

ACKNOWLEDGMENTS

This work was supported by the National Key Research and Development Program of China (grant no. 2022YFA1404304), National Natural Science Foundation of China (grant no. 12204552), and Guangdong Basic and Applied Basic Research Foundation (grant no. 2023B1515040023).

REFERENCES

(1) Ozawa, T.; Price, H. M.; Amo, A.; Goldman, N.; Hafezi, M.; Lu, L.; Rechtsman, M. C.; Schuster, D.; Simon, J.; Zilberberg, O.;

Carusotto, I. Topological photonics. *Rev. Mod. Phys.* **2019**, *91* (1), 015006−015081.
(2) Han, N.; Xi, X.; Meng, Y.; Chen, H.; Gao, Z.; Yang, Y. Topological photonics in three and higher dimensions. *APL Photonics* **2024**, *9* (1), 010902.
(3) Chen, W. J.; Xiao, M.; Chan, C. T. Photonic crystals possessing multiple Weyl points and the experimental observation of robust surface states. *Nat. Commun.* **2016**, *7* (1), 13038.
(4) Yang, Y.; Gao, Z.; Xue, H.; Zhang, L.; He, M.; Yang, Z.; Singh, R.; Chong, Y.; Zhang, B.; Chen, H. Realization of a three-dimensional photonic topological insulator. *Nature* **2019**, *565*, 622−626.
(5) Yang, Y.; Sun, H.-X.; Xia, J.-P.; Xue, H.; Gao, Z.; Ge, Y.; Jia, D.; Yuan, S.-Q.; Chong, Y.; Zhang, B. Topological triply degenerate point with double Fermi arcs. *Nat. Phys.* **2019**, *15* (7), 645−649.
(6) He, H.; Qiu, C.; Ye, L.; Cai, X.; Fan, X.; Ke, M.; Zhang, F.; Liu, Z. Topological negative refraction of surface acoustic waves in a Weyl phononic crystal. *Nature* **2018**, *560* (7716), 61−64.
(7) Lu, L.; Fang, C.; Fu, L.; Johnson, S. G.; Joannopoulos, J. D.; Soljačić, M. Symmetry-protected topological photonic crystal in three dimensions. *Nat. Phys.* **2016**, *12*, 337−340.
(8) Liu, G. G.; Gao, Z.; Wang, Q.; Xi, X.; Hu, Y. H.; Wang, M.; Liu, C.; Lin, X.; Deng, L.; Yang, S. A.; Zhou, P.; Yang, Y.; Chong, Y.; Zhang, B. Topological Chern vectors in three-dimensional photonic crystals. *Nature* **2022**, *609* (7929), 925−930.
(9) Kim, M.; Wang, Z.; Yang, Y.; Teo, H. T.; Rho, J.; Zhang, B. Three-dimensional photonic topological insulator without spin-orbit coupling. *Nat. Commun.* **2022**, *13* (1), 3499.
(10) Slobozhanyuk, A.; Mousavi, S. H.; Ni, X.; Smirnova, D.; Kivshar, Y. S.; Khanikaev, A. B. Three-dimensional all-dielectric photonic topological insulator. *Nat. Photonics* **2017**, *11*, 130−136.
(11) Fang, C.; Weng, H.; Dai, X.; Fang, Z. Topological nodal line semimetals. *Chin. Phys. B* **2016**, *25* (11), 117106.
(12) Hirayama, M.; Okugawa, R.; Murakami, S. Topological Semimetals Studied by Ab Initio Calculations. *J. Phys. Soc. Jpn.* **2018**, *87* (4), 041002.
(13) Armitage, N. P.; Mele, E. J.; Vishwanath, A. Weyl and Dirac semimetals in three-dimensional solids. *Rev. Mod. Phys.* **2018**, *90* (1), 015001.
(14) Yang, B.; Guo, Q.; Tremain, B.; Liu, R.; Barr, L. E.; Yan, Q.; Gao, W.; Liu, H.; Xiang, Y.; Chen, J.; Fang, C.; Hibbins, A.; Lu, L.; Zhang, S. Ideal Weyl points and helicoid surface states in artificial photonic crystal structures. *Science* **2018**, *359*, 1013−1016.
(15) Lu, L.; Wang, Z.; Ye, D.; Ran, L.; Fu, L.; Joannopoulos, J. D.; Soljačić, M. Experimental observation of Weyl points. *Science* **2015**, *349* (6248), 622−624.
(16) Xiao, M.; Ye, L.; Qiu, C.; He, H.; Liu, Z.; Fan, S. Experimental demonstration of acoustic semimetal with topologically charged nodal surface. *Sci. Adv.* **2020**, *6* (8), No. eaav2360.
(17) Yang, Y.; Xia, J. P.; Sun, H. X.; Ge, Y.; Jia, D.; Yuan, S. Q.; Yang, S. A.; Chong, Y.; Zhang, B. Observation of a topological nodal surface and its surface-state arcs in an artificial acoustic crystal. *Nat. Commun.* **2019**, *10* (1), 5185.
(18) Wang, H.-X.; Chen, Y.; Hang, Z. H.; Kee, H.-Y.; Jiang, J.-H. Type-II Dirac photons. *npj Quantum Mater.* **2017**, *2* (1), 54−61.
(19) Gao, W.; Yang, B.; Tremain, B.; Liu, H.; Guo, Q.; Xia, L.; Hibbins, A. P.; Zhang, S. Experimental observation of photonic nodal line degeneracies in metacrystals. *Nat. Commun.* **2018**, *9* (1), 950.
(20) Deng, W.; Lu, J.; Li, F.; Huang, X.; Yan, M.; Ma, J.; Liu, Z. Nodal rings and drumhead surface states in phononic crystals. *Nat. Commun.* **2019**, *10* (1), 1769.
(21) Yang, B.; Bi, Y.; Zhang, R. X.; Zhang, R. Y.; You, O.; Zhu, Z.; Feng, J.; Sun, H.; Chan, C. T.; Liu, C. X.; Zhang, S. Momentum space toroidal moment in a photonic metamaterial. *Nat. Commun.* **2021**, *12* (1), 1784.
(22) Deng, W.-M.; Chen, Z.-M.; Li, M.-Y.; Guo, C.-H.; Tian, Z.-T.; Sun, K.-X.; Chen, X.-D.; Chen, W.-J.; Dong, J.-W. Ideal nodal rings of one-dimensional photonic crystals in the visible region. *Light Sci. Appl.* **2022**, *11* (1), 134.
(23) Yan, Q.; Liu, R.; Yan, Z.; Liu, B.; Chen, H.; Wang, Z.; Lu, L. Experimental discovery of nodal chains. *Nat. Phys.* **2018**, *14* (5), 461−464.
(24) Xiong, Z.; Zhang, R.-Y.; Yu, R.; Chan, C. T.; Chen, Y. Hidden-symmetry-enforced nexus points of nodal lines in layer-stacked dielectric photonic crystals. *Light Sci. Appl.* **2020**, *9* (1), 176.
(25) Hu, S.; Guo, Z.; Jiang, H.; Chen, H. Photonic Dirac nodal-line semimetals realized by a hypercrystal. *Phys. Rev. Res.* **2022**, *4* (2), 023047.
(26) Hu, M.; Zhang, Y.; Jiang, X.; Qiao, T.; Wang, Q.; Zhu, S.; Xiao, M.; Liu, H. Double-bowl state in photonic Dirac nodal line semimetal. *Light Sci. Appl.* **2021**, *10* (1), 170.
(27) Yariv, A.; Yeh, P. *Optical Electronics in Modern Communications*, 6th ed.; Oxford University Press: USA, 2007; Vol. *1*.
(28) Yu, Z.-M.; Zhang, Z.; Liu, G.-B.; Wu, W.; Li, X.-P.; Zhang, R.-W.; Yang, S. A.; Yao, Y. Encyclopedia of emergent particles in three-dimensional crystals. *Sci. Bull.* **2022**, *67* (4), 375−380.
(29) Li, S.; Yu, Z.-M.; Liu, Y.; Guan, S.; Wang, S.-S.; Zhang, X.; Yao, Y.; Yang, S. A. Type-II nodal loops: Theory and material realization. *Phys. Rev. B* **2017**, *96* (8), 081106.
(30) Fang, C.; Chen, Y.; Kee, H.-Y.; Fu, L. Topological nodal line semimetals with and without spin-orbital coupling. *Phys. Rev. B* **2015**, *92* (8), 081201.
(31) Li, T.; Yin, C.; Wu, F. Strong optical non-reciprocity in one-dimensional photonic crystal containing a Weyl semimetal-based defect. *Opt. Mater.* **2021**, *121*, 111583.
(32) Yeh, P. *Optical Waves in Layered Media*; Wiley, 2005.
(33) Dong, J.-W.; Chen, X.-D.; Zhu, H.; Wang, Y.; Zhang, X. Valley photonic crystals for control of spin and topology. *Nat. Mater.* **2017**, *16* (3), 298−302.
(34) Gao, F.; Xue, H.; Yang, Z.; Lai, K.; Yu, Y.; Lin, X.; Chong, Y.; Shvets, G.; Zhang, B. Topologically protected refraction of robust kink states in valley photonic crystals. *Nat. Phys.* **2018**, *14*, 140−144.
(35) Ma, T.; Shvets, G. All-Si valley-Hall photonic topological insulator. *New J. Phys.* **2016**, *18* (2), 025012.
(36) Wu, X.; Meng, Y.; Tian, J.; Huang, Y.; Xiang, H.; Han, D.; Wen, W. Direct observation of valley-polarized topological edge states in designer surface plasmon crystals. *Nat. Commun.* **2017**, *8* (1), 1304.
(37) Kaliteevski, M.; Iorsh, I.; Brand, S.; Abram, R. A.; Chamberlain, J. M.; Kavokin, A. V.; Shelykh, I. A. Tamm plasmon-polaritons: Possible electromagnetic states at the interface of a metal and a dielectric Bragg mirror. *Phys. Rev. B: Condens. Matter Mater. Phys.* **2007**, *76* (16), 165415.
(38) Sasin, M. E.; Seisyan, R. P.; Kalitteevski, M. A.; Brand, S.; Abram, R. A.; Chamberlain, J. M.; Egorov, A. Y.; Vasil'ev, A. P.; Mikhrin, V. S.; Kavokin, A. V. Tamm plasmon polaritons: Slow and spatially compact light. *Appl. Phys. Lett.* **2008**, *92* (25), 251112.
(39) Kavokin, A.; Shelykh, I.; Malpuech, G. Optical Tamm states for the fabrication of polariton lasers. *Appl. Phys. Lett.* **2005**, *87* (26), 261105.
(40) Wu, F.; Wu, J.; Fan, C.; Guo, Z.; Xue, C.; Jiang, H.; Sun, Y.; Li, Y.; Chen, H. Omnidirectional optical filtering based on two kinds of photonic band gaps with different angle-dependent properties. *Europhys. Lett.* **2020**, *129* (3), 34004.
(41) Jia, Y.; Ren, P.; Fan, C. Thermal tunable one-dimensional photonic crystals containing phase change material*. *Chin. Phys. B* **2020**, *29* (10), 104210.
(42) Yue, Y.; Gong, J. P. Tunable one-dimensional photonic crystals from soft materials. *J. Photochem. Photobiol., C* **2015**, *23*, 45−67.
(43) Kosten, E. D.; Kayes, B. M.; Atwater, H. A. Experimental demonstration of enhanced photon recycling in angle-restricted GaAs solar cells. *Energy Environ. Sci.* **2014**, *7* (6), 1907−1912.
(44) Kosten, E. D.; Atwater, J. H.; Parsons, J.; Polman, A.; Atwater, H. A. Highly efficient GaAs solar cells by limiting light emission angle. *Light Sci. Appl.* **2013**, *2* (1), No. e45.
(45) Jeong, E.; Lim, Y. J.; Chin, M. H.; Kim, J. H.; Lee, S. H.; Ji, S. H.; Lee, G. D.; Park, K. H.; Choi, H. C.; Ahn, B. C. Viewing-angle controllable liquid crystal display using a fringe- and vertical-field

https://doi.org/10.1021/acsphotonics.4c00248
ACS Photonics XXXX, XXX, XXX−XXX

driven hybrid aligned nematic liquid crystal. *Appl. Phys. Lett.* **2008**, *92* (26), 705.
(46) Shen, Y.; Hsu, C. W.; Yeng, Y. X.; Joannopoulos, J. D.; Soljačić, M. Broadband angular selectivity of light at the nanoscale: Progress, applications, and outlook. *Appl. Phys. Rev.* **2016**, *3* (1), 011103.
(47) Johnson, S. G.; Joannopoulos, J. D. Block-iterative frequency-domain methods for Maxwell's equations in a planewave basis. *Opt. Express* **2001**, *8* (3), 173−190.

https://doi.org/10.1021/acsphotonics.4c00248
ACS Photonics XXXX, XXX, XXX−XXX